SPIDER: a new balloon-borne experiment to measure CMB polarization on large angular scales

T. E. Montroy, P. A. R. Ade, R. Bihary, J. J. Bock, J. R. Bond, et al.

T. E. Montroy, P. A. R. Ade, R. Bihary, J. J. Bock, J. R. Bond, J. Brevick, C. R. Contaldi, B. P. Crill, A. Crites, O. Doré, L. Duband, S. R. Golwala, M. Halpern, G. Hilton, W. Holmes, V. V. Hristov, K. Irwin, W. C. Jones, C. L. Kuo, A. E. Lange, C. J. MacTavish, P. Mason, J. Mulder, C. B. Netterfield, E. Pascale, J. E. Ruhl, A. Trangsrud, C. Tucker, A. Turner, M. Viero, "SPIDER: a new balloon-borne experiment to measure CMB polarization on large angular scales," Proc. SPIE 6267, Ground-based and Airborne Telescopes, 62670R (12 July 2006); doi: 10.1117/12.670339

SPIE.

Event: SPIE Astronomical Telescopes + Instrumentation, 2006, Orlando, Florida , United States

SPIDER: a New Balloon-Borne Experiment to Measure CMB Polarization on Large Angular Scales

T. E. Montroy[a], P. A. R. Ade[b], R. Bihary[a], J. J. Bock[c], J. R. Bond[d], J. Brevik[e], C. R. Contaldi[f], B. P. Crill[g], A. Crites[e], O. Doré[d], L. Duband[h], S. R. Golwala[e], M. Halpern[i], G. Hilton[j], W. Holmes[c], V. V. Hristov[e], K. Irwin[j], W. C. Jones[e], C. L. Kuo[e], A. E. Lange[e], C. J. MacTavish [d,k], P. Mason[e], J. Mulder[c], C. B. Netterfield[k,l], E. Pascale [k], J. E. Ruhl[a], A. Trangsrud[e], C. Tucker[b], A. Turner[c] and M. Viero[k]

[a]Department of Physics, Case Western Reserve University, Cleveland, OH, USA;
[b]Cardiff University, Cardiff, Wales, U.K.;
[c]NASA, Jet Propulsion Laboratory, Pasadena, CA, USA;
[d]Canadian Institute for Theoretical Astrophysics, University of Toronto, Toronto, Ontario, Canada;
[e]Division of Physics, Math and Astronomy, California Institute of Technology, Pasadena, CA, USA;
[f]Theoretical Physics Group, Imperial College, London, UK;
[g]IPAC, California Institute of Technology, Pasadena, CA, USA;
[h]Commissariat A L'energie Atomique, Paris, France;
[i]Deptarment of Physics and Astronomy, University of British Columbia, Vancouver, BC, Canada;
[j]National Institute of Standards and Technology, Boulder, CO, USA;
[k]Physics Department, University of Toronto, Toronto, Ontario, Canada;
[l]Department of Astronomy and Astrophysics, University of Toronto, Toronto, Ontario, Canada;

ABSTRACT

We describe SPIDER, a novel balloon-borne experiment designed to measure the polarization of the Cosmic Microwave Background (CMB) on large angular scales. The primary goal of SPIDER is to detect the faint signature of inflationary gravitational waves in the CMB polarization. The payload consists of six telescopes, each operating in a single frequency band and cooled to 4 K by a common LN/LHe cryostat. The primary optic for each telescope is a 25 cm diameter lens cooled to 4 K. Each telescope feeds an array of antenna coupled, polarization sensitive sub-Kelvin bolometers that covers a 20 degree diameter FOV with diffraction limited resolution. The six focal planes span 70 to 300 GHz in a manner optimized to separate polarized galactic emission from CMB polarization, and together contain over 2300 detectors. Polarization modulation is achieved by rotating a cryogenic half-wave plate in front of the primary optic of each telescope. The cryogenic system is designed for 30 days of operation. Observations will be conducted during the night portions of a mid-latitude, long duration balloon flight which will circumnavigate the globe from Australia. By spinning the payload at 1 rpm with the six telescopes fixed in elevation, SPIDER will map approximately half of the sky at each frequency on each night of the flight.

Keywords: Radio telescopes, Scientific ballooning, Cosmic Microwave Background Radiation, Bolometer, Polarimetry, Focal plane arrays, SQUID, Half-wave plate

1. INTRODUCTION

For over forty years, the cosmic microwave background radiation (CMB) has provided us with invaluable information about our universe. Its discovery by Penzias and Wilson in 1965[1] provided the first strong evidence for the hot big bang model of cosmology. Experiments on the COBE satellite showed that the CMB spectrum is a nearly perfect blackbody with temperature 2.725 K,[2,3] and that there are intensity anisotropies of order 1 part in 10^5.[4,5] The high degree of isotropy of the CMB has provided support for inflationary theory[6] which says that the early universe went through a period of exponential growth. In recent years, measurements of the angular power spectrum of CMB temperature anisotropies have

Further author information: (Send correspondence to T. Montroy): E-mail: tom@cmb.cwru.edu, Telephone: 1 216 368 2489

Ground-based and Airborne Telescopes, edited by Larry M. Stepp, Proc. of SPIE
Vol. 6267, 62670R, (2006) · 0277-786X/06/$15 · doi: 10.1117/12.670339

played a major role in the development of a cosmological standard model.[7–9] These results tell us that the universe is very close to flat and that $\sim 5\%$ of the energy comes from baryonic matter, $\sim 25\%$ from cold dark matter and $\sim 75\%$ from "dark energy". The apparent flatness of the universe provides further evidence for inflation.

The CMB is polarized via Thomson scattering[10] during recombination and reionization with an amplitude that is less than 10% of the temperature anisotropy signal.[11] Measurements of CMB polarization can tighten current constraints on cosmological parameters as well as providing new independent constraints. We have only recently reached the sensitivity level required to measure CMB polarization.[12–17] These measurements show evidence of an acoustic peak structure predicted by temperature anisotropy measurements, thus supporting the idea that the initial perturbations were adiabatic. The WMAP polarization results on large angular scales[9,17] break parameter estimation degeneracies to provide a constraint on the optical depth to reionization (τ_{reion}). Sensitive measurements on small angular scales have the potential to constrain the neutrino mass, the equation of state of dark energy and to provide new constraints on the nature of reionization. Perhaps, the most exciting prospect is that it may be possible to obtain direct evidence of inflation through its unique imprint on the pattern of CMB polarization.[18,19]

If an unpolarized radiation field incident on an electron has a quadrupole moment in its intensity distribution, then Thomson scattering can produce polarized radiation. The primary source for both temperature and polarization anisotropies is scalar density perturbations in the early universe. While temperature anisotropies correspond to densities on the surface of last scattering, the polarization signal is coupled to velocity fields which create quadrupole moments in the radiation intensity. Temperature and polarization anisotropies can also be sourced by tensor perturbations from gravitational waves, which create intensity quadrupoles by distorting photon wavelengths. The CMB is polarized when the photons scatter for the last time during recombination (any polarization signal produced earlier is washed away by subsequent scattering) and when CMB photons scatter off of free electrons after the universe is later reionized.

It is customary to characterize CMB polarization as the sum of two rotational invariant components: E-modes and B-modes.[20,21] In analogy to electromagnetism, E-modes are curl-free while B-modes are divergence-free. They are related to the Stokes Q and U parameters via a non-local linear transformation - the CMB is not expected to be circularly polarized so Q and U completely characterize CMB polarization. Scalar density perturbations only produce E-mode polarization, while gravitational waves produce roughly equal parts E-mode and B-mode polarization.[22]

Most inflationary theories predict a spectrum of primordial gravitational waves[18,19] and the amplitude of its imprint on the CMB is related to the energy scale at the time of inflation.[23] Although the gravitational waves produce temperature anisotropies, their presence is masked by presence of anisotropies produced by scalar fluctuations; the E-mode angular power spectrum is similarly dominated by the scalar component. Only a measurement of the angular power spectrum of B-mode polarization has the potential to provide a clean measurement of the contribution from inflationary gravitational waves.

As shown in Figure 1, the CMB polarization signal from gravitational waves is expected to be very weak: roughly 1000 times smaller than the temperature anisotropy signal and a factor of several smaller than the scalar E-mode signal. This places strong requirements on experimental sensitivity and systematic error rejection. To further complicate matters, the gravitational wave B-mode signal could be confused by polarized galactic emission and by gravitational lensing which converts primordial E-mode polarization into B-mode polarization.[24] In addition, the conversion from Stokes parameters Q and U to E-modes and B-modes can lead to a loss of signal for spatial modes that exist near the boundaries of the survey region.[25,26]

In this paper, we present SPIDER, a novel balloon-borne payload for observations of polarized radiation at millimeter wavelengths. SPIDER is designed to provide high-fidelity measurements of CMB polarization and galactic dust emission on angular scales greater than 1° over 50% of the sky. It is both a science and technological pathfinder for a potential future satellite mission to measure CMB polarization. SPIDER will have the sensitivity to place strong constraints on the E-mode polarization signal on large angular scales; thereby, tightening constraints on the optical depth to reionization. SPIDER will provide a large scale survey of polarized dust emission at millimeter wavelengths. In the absence of foreground emission, SPIDER will measure or place strong upper limits on the gravitational wave B-mode signal with a sensitivity that is roughly eight times better than current limits.[9]

In Section 2, we discuss the SPIDER's science goals in more detail. In Section 3, we discuss the architecture of the SPIDER payload, the choice of frequency bands and the advantages of using a balloon-borne platform for CMB observations. We then discuss the telescope components in more detail: the optical design is discussed in Section 4, detectors

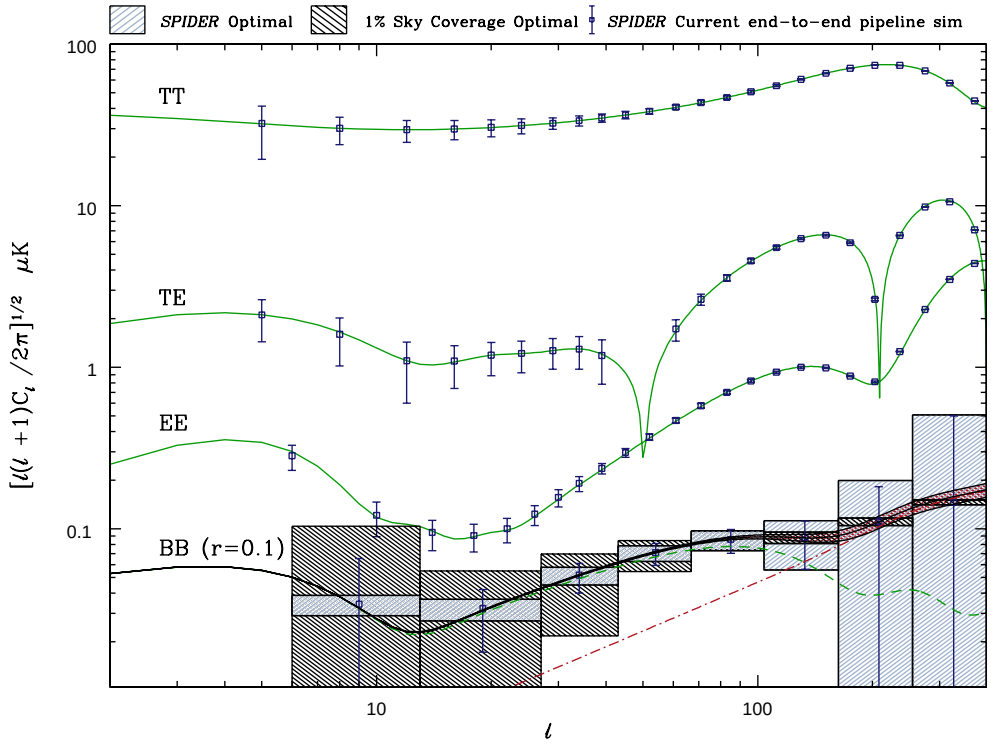

Figure 1. The accuracy with which SPIDER will measure the TT, TE, EE and BB power spectra. The data with error flags are the average results of extensive simulations using the XFASTER[27] pipeline on 200 end-to-end realizations of a simulated SPIDER flight, observing a fiducial CMB sky model ($r = 0.1$, $\tau = 0.1$). These simulations included the effects of $1/f$ noise and gain drifts in the detector system, finite wave plate rotation speed, and finite sky coverage. For the measurements of the BB spectrum on large angular scales, non-optimal separation of E-mode and B-mode spectra by the current pipeline leads to excess uncertainty.[25,26] Straightforward modifications to the existing pipeline will result in the improved accuracy indicated by the light error boxes labeled "SPIDER Optimal". The optimal errors properly account for the loss of modes induced by the apodization of the mask (in this case a 10° $\cos^2$ edge apodization of a $|b| < 15$ galaxy cut) and finite pixelization. The dark error boxes are the optimal errors for a survey covering 1% of the sky (e.g. EBEX[28]) with a similar number of detectors and amount of integration time; those errors are computed on a circular cap covering 1% of the sky with a 5 degree circular apodization. Separate primordial (long dash) and lensing (dot dash) contributions for the total BB signal are also shown and the shaded contours around the mean BB model show the effect on the high-ℓ signal of a 20% uncertainty in the lensing contribution. SPIDER excels in the region where uncertainty in the lensing model is least important.

and readout electronics are discussed in Section 5, and the cryostat is discussed in Section 6. In Section 7, we discuss the control of systematic errors.

2. SCIENCE GOALS

SPIDER will provide sensitive, high-fidelity, multi-frequency maps of polarization covering more than 50% of the sky. This data will have a strong impact on our understanding of cosmology and the galaxy. SPIDER's three primary science goals are to (i) determine the optical depth to scattering of CMB photons since reionization, (ii) search for B-mode polarization from inflationary gravitational waves, and (iii) to characterize millimeter-wave polarized emission from interstellar dust.

2.1. Reionization

SPIDER's measurement of the angular power spectrum of E-mode polarization on large angular scales will place a strong constraint on the optical depth to reionization (τ_{reion}) which will help in the understanding of early star formation. A variety of astrophysical observations indicate that the universe was mostly ionized by a redshift of $z \sim 6$.[29–31] When CMB

photons scatter off of reionized electrons, the polarization signal is amplified on spatial scales corresponding to the horizon size at that time. On large angular scales (corresponding to multipole moments $\ell = 2-6$), the three year WMAP results[17] detect a signal in the E-mode power spectrum which implies that reionization occurred at a redshift of $z \sim 10.5$ and that $\tau_{reion} = 0.09 \pm 0.03$. As shown in the left panel of Figure 2, SPIDER will be able to significantly tighten constraints on τ_{reion} - more than a factor of three better than the expected results from eight years of WMAP observations.

2.2. Inflationary Gravitational Waves

The amplitude of the inflationary gravitational wave signal is characterized by the tensor-to-scalar ratio r. It is conventionally defined as the ratio of the power in primordial tensor fluctuations to the power in primordial scalar fluctuations at the wavenumber $k_0 = 0.002$ Mpc^{-1}.[32] The current limit is that $r_{0.002} < 0.3$ (95% C.L.),[9] and if the energy scale of inflation is near to the energy scale of grand unification, it is likely that $r_{0.002} > 0.01$. Besides its small amplitude, detection of the B-mode gravitational wave component is complicated by three additional factors: polarized foreground emission, gravitational lensing of E-mode polarization into B-mode polarization,[24] and the potential for mixing between E-mode and B-mode polarization when only part of the sky is observed.[25,26] For SPIDER the frequency bands have been chosen to optimize the separation of galactic emission from CMB polarization. By covering a large portion of the sky and focusing on angular scales larger than 1°, SPIDER is relatively immune to the effects of gravitational lensing and E-B mixing. Figure 1 and the left panel of Figure 2 show expected results for SPIDER if $r_{0.002} = 0.1$. In the absence of foreground emission, SPIDER will detect gravitational waves at the level of $r_{0.002} = 0.04$ (3σ).

2.3. Polarized Dust Emission

As the recent WMAP results show,[17] galactic emission is a significant component of the polarized signal at millimeter wavelengths, especially on large angular scales. The primary sources of polarized emission on these scales are synchrotron emission, which dominates for $\nu < 70$ GHz, and thermal dust emission, which dominates at higher frequencies. While results from continued WMAP observations will provide strong constraints on synchrotron polarization, SPIDER is uniquely positioned to characterize polarized dust emission. Both synchrotron and dust polarization are influenced by the galactic magnetic field; however, synchrotron probes the relatively low density regions of the interstellar medium (ISM) while dust emission probes a wider density range. The WMAP synchrotron data provides confirmation that a relatively simple bisymmetric spiral model explains the gross magnetic field structure in the galaxy, but the role of magnetic fields in star formation and other processes in the dense ISM is not well understood. SPIDER data on large angular scales will complement high resolution measurements from ground based telescopes and optical measurements of starlight polarization in the galactic plane (currently the primary probe of polarized dust emission). In addition, the SPIDER maps can be used to study high-latitude clouds and infrared cirrus, thus providing information about the "local" ISM.

3. SPIDER

3.1. Payload Design

Figure 3 shows the design of the SPIDER payload. SPIDER consists of six single frequency telescopes operating in bands centered at frequencies of 80, 100, 145, 225 and 275 GHz (two telescopes operate at 100 GHz. Each telescope consists of a 25 cm primary optic cooled to 4 K. Incoming polarized radiation is modulated by a rapidly rotating half-wave plate (HWP) placed in front of the primary optic and cooled to 20 K. The optical chain couples incoming radiation onto arrays of polarization sensitive, antenna coupled, transition edge superconducting (TES) bolometers. There are over 2300 detectors, readout with time-domain SQUID multiplexing, spread among the six telescopes. All six telescope inserts are housed in a single LN/LHe cryostat which has been designed for a 30 day hold time. The detectors are cooled to 300 mK using a simple He^3 closed cycle refrigerator, one per insert.

All aspects of the SPIDER design have been optimized to be robust, easily characterizable and to mitigate potential sources of systematic errors. The payload spins continuously in azimuth while observing at a fix elevation; this reduces the potential for correlated noise due to payload accelerations at the end of a scan. The on-axis telescope design has a low susceptibility to optically induced systematic errors, and housing the telescope at 4 K mitigates environmental effects. Placing the rapidly rotating HWP in front of the primary optic greatly reduces the potential for systematic errors in the reconstruction of polarized maps. The small size of the telescope aperture puts the far-field of the telescope relatively nearby (30 m); this allows for complete characterization of the telescope beam response before flight using a ground based

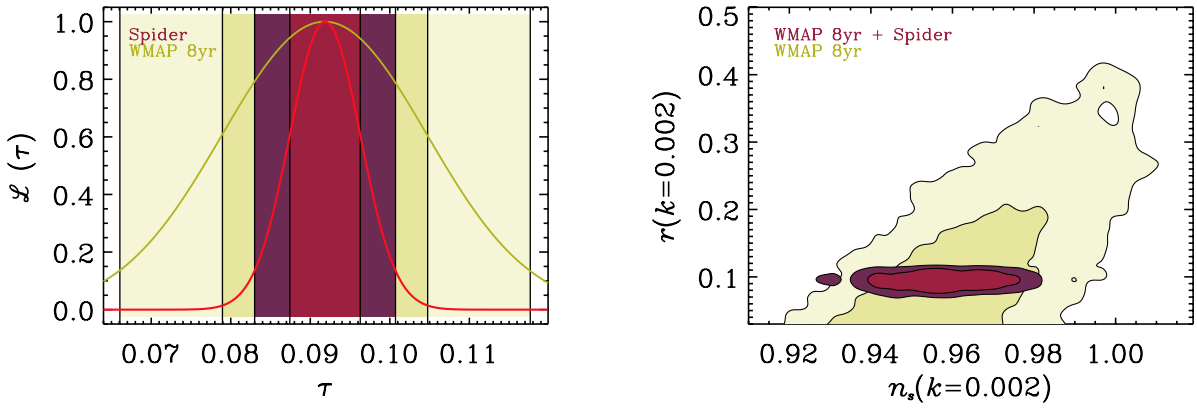

Figure 2. *Left:* Relative likelihood of τ_{reion} as measured by SPIDER C_ℓ^{EE} only (dark curve) and WMAP-8yr only (light curve). The vertical lines represent the 1σ and 2σ errors. SPIDER improves over the expected WMAP 8-yr constraints by more than a factor of three. The SPIDER likelihood is the exact likelihood of the C_ℓ^{EE} as computed from end-to-end pipeline simulations, using only the 100 GHz channels. *Right:* Likelihood contours (for the 68% and 95% confidence levels) in the n_s–r plane obtained by WMAP-8yr only (light contours) and WMAP-8yr & SPIDER (dark contours). Constraining r allows SPIDER to break one of the more severe degeneracies remaining in the CMB data. The SPIDER constraints on τ_{reion} and r represent a reduction in the allowed volume in the n_s-τ-r parameter space by a factor greater than 50.

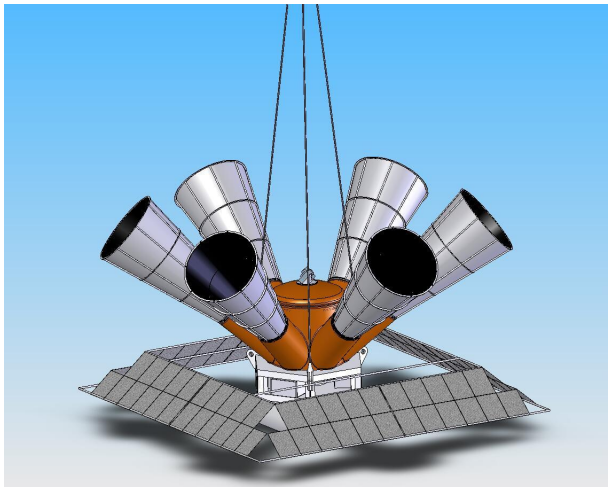

Figure 3. The SPIDER payload is designed to obtain maximum sky coverage during the night portions of a 25 day mid-latitude circumnavigation of the Earth. The entire payload is rotated in azimuth at $6^\circ/s$, scanning each of the 6 single frequency telescopes around the sky once per minute. Each telescope is fully baffled from radiation emitted or reflected by the ground or the balloon. A pair of star cameras mounted on the top of the cryostat will allow pointing reconstruction with $\sim 6''$ precision. The control and data acquisition electronics are conveniently mounted below the cryostat surrounding a small azimuth reaction wheel, and above the CSBF SIP electronics. Up to 2000lbs of ballast is suspended below the SIP.

source. In addition, a long baffle can be deployed that completely surrounds the aperture and prevents direct or reflected illumination by either the balloon or Earth's limb.

Given the azimuthal symmetry of the payload, SPIDER must make observations only when the sun is below the horizon. The daytime portion of the flight will be used to re-charge the batteries using an array of solar panels and to re-cycle the He^3 refrigerators. On each night of observation, SPIDER will map a nearly identical patch on the sky. The accessible sky

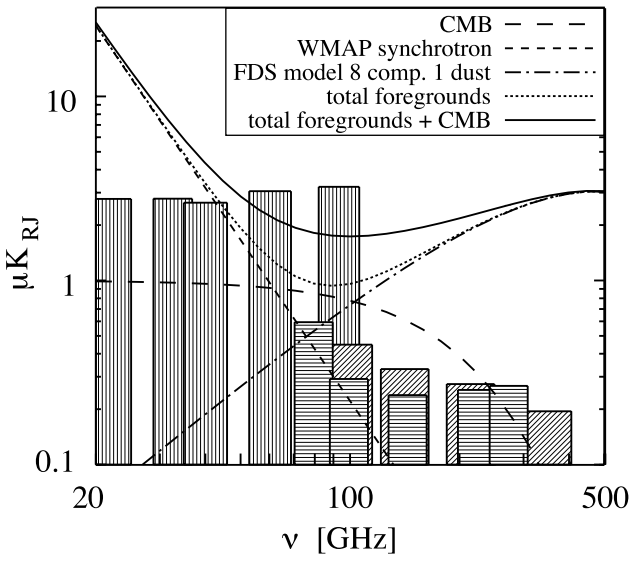

Figure 4. Frequency dependence of galactic emission and the CMB compared with the WMAP (vertical hatch), SPIDER (horizontal hatch), and *Planck* (slanted hatch) bands. The heights of the bands correspond to the per-pixel rms instrumental noise for 14' pixels.

region depends on the payload trajectory; however, deviations from a constant latitude flight will increase the sky coverage and the amount of cross-linking in the maps. Figure 5 shows the expected sky coverage for a single day of observations and a map of Galactic dust emission measured by IRAS.

3.2. Choice of Frequency Bands

The polarization signal from galactic foreground emission is likely to be a significant source of contamination for CMB polarization measurements on large angular scales. Thus, observations at multiple frequencies are needed in order to separate the galactic polarization signal from CMB polarization. For SPIDER we expect that we will need to subtract $\sim 90\%$ of foreground polarization in order for instrument noise to dominate. The expected WMAP 8 year results will provide constraints on synchrotron at frequencies below 65 GHz similar to those achievable by SPIDER (given SPIDER's payload constraints). Therefore, we plan to use the WMAP data to remove synchrotron and allocate SPIDER's bands to constrain the dust component. To determine the optimal band allocation, we performed a series of simulations using expected WMAP 8 year sensitivities, expected SPIDER sensitivities and a realistic model of galactic emission. Given the dust spectrum and instrumental noise constraints (both pixel counts and atmospheric noise increase with frequency), the candidate bands were 225, 275, 350 and 450 GHz. Figure 4 shows the CMB and foreground signals as a function of frequency along with the bands and pixel noise for SPIDER, WMAP and *Planck*.[33,34]

In our simulations, we use a method similar to that used in Eriksen et al.:[35] first fit for non-linear model parameters (power-law indices and dust temperature) on large pixels, then spatially smooth the nonlinear parameter fields and fix them when fitting the linear amplitudes in small pixels. The properties of dust emission at frequencies below 300 GHz are not well constrained, and both the dust temperature (there may even be more than one thermal component) and emissivity spectral index are expected to vary across the sky.[36] Given SPIDER's expected sensitivity at these frequencies, we find that it is difficult to simultaneously determine the dust temperature and spectral index (even for a single temperature component) on any spatial scale smaller than entire map. Using a dust temperature map ("FDS model 8") from Finkbeiner et al.[36] and fitting only for the spectral indices, we find that we can measure galactic emission to the required 10% precision on maps smoothed with a 30° window. Keeping the nonlinear parameters fixed, we recalculate the linear parameters on 2° pixels and find that the our precision on the CMB is 40% less than it would be without galactic emission. Although the 350 and 450 GHz bands would result in a higher signal-to-noise measurement of dust polarization, we choose to operate at 225 and 275 GHz because the extrapolation of data at these frequencies down to lower frequencies is less sensitive to variations in the dust temperature and emissivity spectral index.

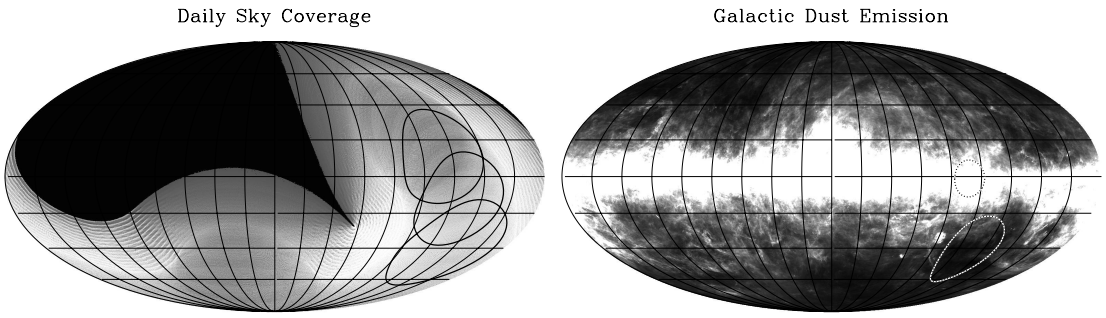

Figure 5. SPIDER sky coverage. The left panel shows the sky coverage for 16 detectors spread over the array's range in elevation (30° to 50° from the horizon). Nearly all of the coverage is repeated each night of the $\sim$ 25 day flight, and the circular scan strategy provides good cross-linking. The three traces show the path of a pixel at the inner edge of the focal plane for a single rotation of the SPIDER gondola, each separated by two hours. SPIDER will map most of the sky accessible from either Antarctica or Chile. For reference, the right panel shows the IRAS 100 μm map of Galactic dust. The outlined areas indicate the fields targeted during the 2003 flight of BOOMERANG.[38] *The larger of the two areas represents the total amount of low foreground sky accessible to an Antarctic LDB flight.*

3.3. Advantages of the Balloon-borne Platform

A balloon flight is an attractive platform for CMB and galactic polarization on large angular scales. Over SPIDER's frequency range, achievable detector sensitivities (Table 1) are more than a factor of two higher than what is possible with background limited detectors at the South Pole.[37] In terms of raw sensitivity, a 20 night balloon flight would be roughly equivalent to 100 days of South Pole observations (1/2 of a winter season) with the same number of detectors and to one year of observations by the orbital mission *Planck* which has far fewer detectors and less immunity to polarization systematics. However, for a ground based measurement, atmospheric inhomogeneities will cause excess noise that further limits measurements on large angular scales. This atmospheric contamination increases strongly with frequency and could drastically reduce the effectiveness of the 225 and 275 GHz channels which are vital for foreground characterization. In addition, the engineering requirements for a balloon-borne payload are similar to those for an orbital mission, thus making SPIDER a potential model for a future CMB orbital mission.

SPIDER must observe with the sun below the horizon and must be able to cover a large area of the sky repeatedly in a single flight. This rules out summer launches of conventional LDB flights from the Antarctic or from Kiruna, Sweden, which are daytime only. The SPIDER baseline plan is a constant latitude flight around the world, launched from Alice Springs, Australia. Based on decades of experience launching from Alice Springs, high level and surface weather define a two month launch window centered on December 15. The Columbia Scientific Ballooning Facility (CSBF) has simulated in detail the flight track and altitude variations for the SPIDER payload mass launched from Alice Springs (25.5° S Lat, 128.5° E Lon) in early December. Of 75 flights, 69 (92%) returned to Australia in 25.0 ± 4.8 days, while 2 narrowly missed the continent and would have been easily recovered off the coast (SPIDER is designed for a water recovery). The remaining 4 (5%) went outside the bounds (between the equator and $\sim 40^\circ$S) of the simulation. A success rate of 95% is as good as ballooning gets.

4. OPTICAL DESIGN

4.1. Telescope Design

The optical design, shown in Figure 6, represents a minimal modification to the well-characterized *Robinson* (formerly BICEP) telescope.[39] The monochromatic, telecentric refractor uses anti-reflection coated polyethylene lenses and is cooled to 4 K in order to reduce the instrumental background to negligible levels. An apodized, 4 K Lyot-stop smoothly tapers the aperture field distribution of the primary, providing exquisite control of both the near and far side lobes. The primary lens has a diameter of 250 mm, and the clear aperture of the Lyot stop is 200 mm which produces a 40′ beam at 145 GHz. A rotating half-wave plate operating at 20 K is placed in front of the Lyot stop.

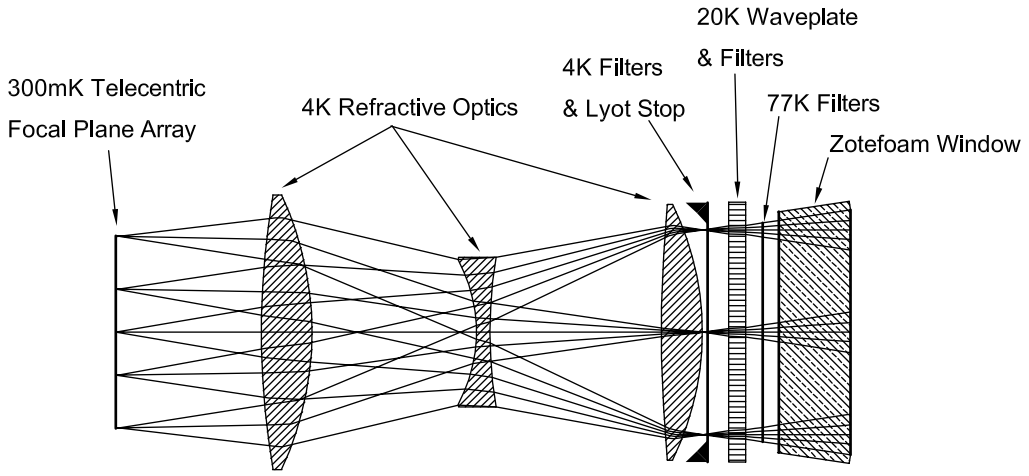

Figure 6. SPIDER optical train. The telescope yields a flat and telecentric focal plane. The three lenses are maintained at 4 K with an apodized Lyot stop (also at 4 K) in front of the primary lens. A 20 K half-wave plate modulates the polarization signal before it reaches the Lyot stop. Lowpass filters are placed on the 4 K, 20 K and 77 K stages to intercept thermal radiation. The vacuum window is made from closed-cell polypropylene foam.

The telescope provides a 20° field of view (FOV) imaged onto the focal plane. Averaged over the full bandwidth, the un-obstructed and azimuthally-symmetric optics result in a negligible contribution to cross-polarization, and produce less than 0.8% instrumental polarization at the outside edge of the field of view. The cross-polar beam response is dominated by the performance of the planar feed antennas, and is significantly mitigated by the apodized 4 K stop.

A combination of reflective metal mesh and lossy PTFE optical filters intercept thermal radiation at the 77 K stage, ^{4}He vapor-cooled stages and the 4 K Lyot stop. These filters limit the radiative heat load on the primary lens, the Lyot stop and the half-wave plate. The 300-mm diameter, low loss vacuum window (95-mm of closed-cell polypropylene foam) provides an unobstructed view from the cold stop.

4.2. Half-wave Plate

Experiments without active polarization modulation such as BOOMERANG03 and *Planck*, nominally measure polarization by differencing the signal from orthogonally oriented polarization sensitive bolometers (PSB's) which reside at the back the same feed structure. Sky rotation may modulate the polarization signal somewhat, but not necessarily enough to make clean measurements of either the Q or U Stokes parameters using a single detector. To measure polarization with high fidelity in this manner, both detectors in a PSB pair must be accurately characterized in terms of gain, frequency response, instrumental polarization and polarization orientation. By modulating the polarization signal, it is possible to measure Q and U with a single detector, thereby significantly reducing the requirements for individual detector characterization. Common techniques for polarization modulation include a half-wave plate or Faraday rotator in the optical chain, or MEM or SIS switches on transmission lines which travel from an antenna to the detector. If the polarization modulator is placed after the primary optic (i.e. closer to the detectors), polarization fidelity will be ultimately limited by differences between the beams produced by each polarization -this is a general feature of nearly all polarized feed systems. The quadrupolar component of the beam mismatch is indistinguishable from a true polarization signal on the sky.[40]

For SPIDER, we have chosen to place a rapidly rotating half-wave plate (HWP) at the aperture of each telescope. Rotating a HWP in front of the primary optic rotates the polarization sensitivity on the sky at four times the physical rotation rate of the wave plate itself, while leaving the beams unchanged. In addition to reducing the potential for systematic errors due beam mismatch, instrument mis-characterization and other systematic errors (see Section 7 for more details), the rapidly rotating HWP modulates the polarization signal at a frequency much higher than the sky signal modulation produced by the scan rate, thereby greatly reducing the requirements on the low frequency stability of the detector.

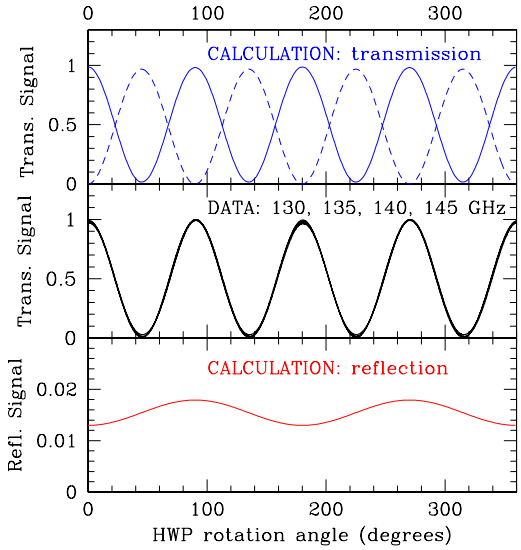

Figure 7. *Top:* The band averaged signal for a pure linearly polarized input vs. rotation angle for a sapphire half wave plate, anti-reflection coated with a single layer of Herasil quartz on each face. A 25% band centered at 150 GHz is used. The solid line is for a detector polarized in the same direction as the input signal, while the dashed line is for a detector polarized orthogonally to the input. The polarization modulation efficiency is near unity (96.8%) in each detector. *Middle:* Laboratory measurements of signal vs. plate rotation angle for a Herasil AR-coated sapphire wave plate (equivalent to the solid line in the top panel, but at specific individual frequencies in the band), as baselined for SPIDER. The polarization modulation is near unity. *Bottom:* Calculated band-averaged reflection vs. rotation angle for the same HWP system. The plotted reflection signal is the sum of both reflected polarizations, for a single input polarization. Note that the reflection signal is modulated at two times the rotation rate of the wave plate, rather than at the signal frequency (four times the rotation rate) as seen in the top panel.

Optical performance

SPIDER's use of single-frequency telescopes makes the HWP design and implementation simple. A single birefringent sapphire wave plate coated with a single layer of Herasil quartz on each side gives very good (band average of 96.8% modulation efficiency) performance over 25% bandwidth. The calculations shown in Figure 7 match boundary conditions in E and H (in each polarization) at the various interfaces, and therefore include the effect of coherent reflections at each interface. An improvement in polarization modulation efficiency (to 99.9%) can be achieved by using multiple stacked sapphire plates,[41,42] but this comes at a cost in internal reflections, phase differences in the $4f$ signal across the photon frequency band, and significant cost (for SPIDER's optics, each 30cm sapphire plate is $\sim$\$10K).

Figure 7 also shows a calculations of the reflected signal as a function of plate rotation angle; such reflections modulate the photon loading on the bolometers (causing a signal), and also lead to instrumental polarization. Fortunately, effects from these reflections appear at $2f$, and so can be easily separated from the true ($4f$) polarization signal from the sky. Nonetheless, to minimize the effects of the reflections seen by the detectors we will operate the HWP at 20 K, just in front of the 4 K pupil. Wave plate reflections will thus be directed to 4 K surfaces, minimizing their impact.

A 10 cm diameter prototype HWP system has been assembled and tested with a tunable Gunn Oscillator and Diode detector. Transmitted signal vs. rotation angle curves at several photon frequencies are shown in the middle panel of Figure 7. The amplitude of each curve is normalized to unity, so the polarization modulation efficiency information lies in the degree to which each curve approaches zero at the minima. Over the tested frequency range the HWP clearly performs very well.

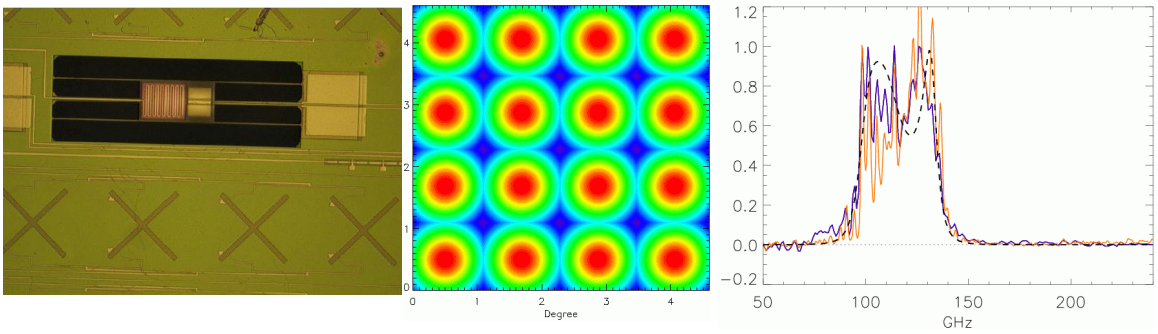

Figure 8. *Left*: Closeup on an antenna-coupled TES bolometer. 4 antennae elements, part of a summing tree, a microstrip filter, the meandering microstrip termination, and the TES are shown. *Middle*: The beams on the sky produced by part of the 100 GHz focal plane. The beam is represented by the Fourier transform of a *measured* antenna angular response, with a -20dB edge taper. The ellipticity is approximately 2%. The array makes efficient use of the large field of view of a telecentric refractive optics. *Right:* The measured spectra of microstrip lumped element filters (solid lines), overplotted with the calculated transmittance (dashed line).

Observing Band (GHz)	Bandwidth (GHz)	Beam FWHM (arcmin)	Number of Spatial Pixels	Number of Detectors	Single-Detector Sensitivity ($\mu K_{CMB}\sqrt{s}$)	Instrument Sensitivity ($\mu K_{CMB}\sqrt{s}$)
80	19	72	100	200	110	7.8
100	24	58	(2×)144	(2×)288	100	4.2
145	35	40	256	512	100	4.4
225	54	26	256	512	204	9.0
275	66	21	256	512	351	15.5

Table 1. Observing bands, pixel and detector counts, and single-detector and instrument sensitivities. The latter is obtained by dividing the single-detector sensitivity by $\sqrt{N_{det}}$. A total of 2312 detectors are distributed between the six telescopes, with two telescopes operating at 100 GHz.

Rotation

The HWP will be rotated at $\sim$ 10 Hz. To rotate (cryogenically) at this speed, the HWP will be suspended on a superconducting magnetic bearing and driven by an AC synchronous motor. The magnetic bearing design is similar to what is being designed for EBEX,[28,43] and is used to minimize the heat load on the liquid helium bath. The wave plate and its drive will be mounted from the 20 K vapor-cooled shields, which allows $\sim$ 500 mW of cooling power per wave plate assembly. Optical testing completed under controlled thermal loading conditions indicates that radiative cooling of the wave plate will maintain this system at temperatures below 30 K. The drive system uses an AC synchronous variable reluctance motor, which uses coils and pole pieces on the stator to apply torque to high permeability plugs on the rotor. This design does not have permanent magnets on the rotor, and thus drastically reduces time-varying magnetic fields which could interfere with the SQUID multiplexer readouts. A room temperature prototype of this system was constructed and used to drive a rotor on an air bearing; based on that experience, a low temperature version using a magnetic bearing is currently under construction.

5. DETECTORS

SPIDER will use polarization sensitive, antenna-coupled bolometers[44,45] (ACB's) operating at a base temperature of 300 mK. Figure 8 shows an image of a prototype detector, the measured beam response and both the expected and measured spectral response. Each spatial pixel consists of a 16×16 phased array of slot dipole antennae. The pixel's radiation pattern is defined by the coherent interference of the antennae elements, yielding a $\sim 13^\circ$ FWHM beam with a first sidelobe at -15 dB when the 256 elements are fed with equal weights. With the sidelobes terminated at the 4K cold stop, the antenna array defines highly symmetrical beams on the sky, with low sidelobes.

Each spatial pixel has two orthogonally polarized antennae. The optical power is transmitted via superconducting microstrips[46] to superconducting transition-edge sensors (TESs) immediately adjacent to the spatial pixel.[47,48] TESs have strong electro-thermal feedback and low heat capacity which lead to an extremely linear and fast bolometer.[49–52] Thermal isolation of the TES films is provided by Si_3N_4 support legs. Optical power is deposited in the TES by terminating the superconducting microstrip with a long Au meander on the same thermal island as the TES.

The array design has a bandwidth of about 25%, set by the slot length. Optical band definition is provided by a combination of in-line lumped element Chebsyshev filters[53] and cryogenic metal mesh filters, the combination of which provide sharp band edges and no intrinsic out-of-band response.

The antenna-coupled design is entirely photolithographically fabricated, greatly simplifying production. No manual steps – such as attachment of semiconductor thermistors or single-pixel lenses – are required. The integrated components are mechanically robust, and immune to differential thermal contraction. The densely populated antennae allow for very efficient use of the focal plane area.

The antenna-coupled architecture has already been demonstrated.[47,48] We have thoroughly characterized a series of end-to-end prototype detectors.[45] Radiation patterns have been measured with both optically modulated thermal sources and monochromatic sources, confirming the theoretical predictions. The in-line filters show very sharp cut-off edges and excellent repeatability (Figure 8). To test the reliability of the long summing trees, we have fabricated a test device in which a 5μm-wide microstrip is shown to have no breaks or shorts over its entire length of 255 mm and 3,800 step cross-overs. Furthermore, the prototype detectors have been observed to respond with the expected optical efficiency to a blackbody calibrator, confirming the low microstrip loss demonstrated in our previous work.[46] We currently are developing elemental titanium films for the TES, although Mo/Au, Mo/Cu[54] and Al/Mn alloy[55] films are also being tested.

The distribution of the pixels and the per-pixel sensitivities are indicated in Table 1. In the prime science bands at 100 and 145 GHz, the noise is dominated by and receives approximately equal contributions from the photon and phonon noise components. The contribution from both Johnson noise and amplifier noise is negligible.

The TES sensors will be read out using superconducting quantum interference device (SQUID) current amplifiers with time-domain multiplexing[56–59] to be provided by NIST. Time-domain SQUID multiplexing has been under development for a number of years and is now a fairly mature technology. A scheme quite similar to the one planned for SPIDER is in development for the SCUBA2[60] sub-millimeter camera on the James Clerk Maxwell Telescope. The SCUBA2 room-temperature readout electronics will be adapted with essential no changes for SPIDER.

6. CRYOGENICS

The cryostat for the SPIDER instrument will use liquid nitrogen (LN_2) and liquid helium-4 (LHe) to provide 30 days of cooling power to the instrument. All six instrument inserts and the $\sim$ 200 liter LHe and LN_2 tanks will be contained in an outer vacuum vessel (see Fig. 3) designed by Redstone Aerospace. While the primary LHe tank will be maintained at atmospheric pressure, a small ($\sim$ 25liter) secondary LHe tank will be controlled at a vapor pressure equivalent to an altitude of 80,000 ft. This will provide extremely stable 4 K and 1.5 K operational environments for the telescope and sub-K cooler. The inserts and the liquid cryogen tanks will be surrounded by concentric vapor-cooled shields and the inner tank will be mechanically supported by fiberglass straps. The use of staged vapor cooled shields and radiation blockers reduces the radiative loading on the optics and detectors. Simple and robust closed-cycle ^{3}He refrigerators, similar to that flown on BOOMERANG, will be used to cool the detectors to 300 mK from the 1.5 K base temperature.

7. CONTROL OF SYSTEMATICS

One of the greatest challenges of measuring B-mode polarization at the level targeted by SPIDER is the control of systematic effects. The polarization signal from inflationary gravitational waves is expected to be more than 1000 times weaker than the CMB temperature anisotropies, and a factor of at least several lower than the E-mode polarization anisotropies generated by density perturbations. Measuring this signal therefore requires very good control of various systematic effects related to the instrument itself.

The design of SPIDER has been optimized with these systematic effects in mind. By targeting large angular scales, SPIDER is able to use compact optics, allowing for precise measurements of the relevant beam and polarization characteristics pre-flight. The antennas, filters, and bolometers are fully integrated on the silicon wafers, and the optics are cryogenic and

Parameter	**Effect**	SPIDER **design rms**	**Comments**
Cross-Polar Beam response	$E \rightarrow B$	< 1 nK	Optical design calculations
Main lobe quadrupolar mismatch	$dT \rightarrow B$	< 2 nK	Calculated beam & HWP
Polarized sidelobes on Galaxy/Earth/Moon	$dT \rightarrow B$	< 5 nK	Robinson beam on Earth/Moon/Galaxy
Instrumental Polarization	$dT \rightarrow B$	< 10 nK	Optical calculations & HWP
Relative detector gains	$dT \rightarrow B$	-	HWP
Polarization angle	$E \rightarrow B$	< 6 nK	Measure to 0.5° absolute
Relative detector pointing	$dT \rightarrow B$	-	HWP
Absolute pointing	$E \rightarrow B$	< 3 nK	Determine to $< 1'$ absolute
Total (quadrature sum)		< 14 nK	

Table 2. Potential systematic effects relevant to SPIDER; the effects and estimates are discussed in more detail in the text. For $r = 0.1$, the *rms* B-mode signal is roughly 100 nK, and scales as $\sqrt{r}$. We expect SPIDER to be limited by statistics and galactic foregrounds, rather than systematics, in its ability to detect the polarization signal from gravitational waves.

under vacuum; parameters related to these components will be extremely stable, even if the gondola's thermal environment changes. The optical design and phased-array feeds provide very low cross polarization. The use of a rotating half-wave plate as a polarization modulator, placed in front of the beam forming optics, vastly decreases the level of many systematic effects. Table 2 provides a summary (modeled after Table 6.1 in the report from the Task Force on CMB Research[61]) of the relevant systematic effects and the level at which we expect to control them in SPIDER. Below, we discuss in more detail these effects and our design choices that minimize them; the main point, however, is that SPIDER is designed to be limited by statistics and foregrounds, rather than systematics, in its ability to detect the inflationary signal.

Cross-polar beam response, integrated over the beam pattern, can cause E-B mixing.[62,63] Calculations indicate the planar antennas used by SPIDER provide high rejection to such cross-polar response ($\approx 10^{-4}$), while the on-axis refractive optics produce a very small cross polarization ($\approx 10^{-5}$) even for the off-axis pixels.

Differential Beam ellipticity can mix T (CMB temperature) and E-mode anisotropies into B, with symmetries that otherwise make discrimination of the effect indistinguishable from a true polarization signal on the sky. The planar antennas in SPIDER are calculated to produce co-polar beams with low ellipticity (2-3% max). Hu, Hedman, and Zaldarriaga[62] (hereafter, HHZ) show that a 0.2% integrated quadrupolar mismatch with 1° degree beams, is required to keep the induced B-mode contamination a factor of two below the gravitational lensing B-mode signal over our range of angular scales. For any feed/optical system, this is a challenging requirement. However, the HWP in SPIDER modulates the polarization orientation without affecting the beam shapes, thereby removing sensitivity to beam ellipticity. We also note that the compact telescope design enables a full characterization of these beam mismatches prior to flight.

Polarized sidelobes on the Galaxy. We have simulated the response of our well-baffled antennas, using *Robinson*'s measured beams as a guide, and found that the response to Galactic emission is negligible for $|b| > 20^\circ$.

Instrumental Polarization. We expect roughly 1% instrumental polarization from our optics; however, the HWP, rotated at a frequency f, greatly mitigates this effect. The HWP itself creates a $2f$ instrumental polarization signal, which is easily separated from the real $4f$ polarization sky signal. Assuming the HWP reduces instrumental polarization effects by a factor of 100 yields the 10 nK rms quoted in Table 2.

Relative detector gains. The use of the rotating HWP means that SPIDER determines the polarization signal on the sky from each detector individually; detectors are not differenced, so there is no contamination from relative detector gain errors. We have verified our insensitivity to relative gain errors with a full time stream to power spectrum simulation of SPIDER while including a 0.4% relative gain uncertainty between detectors (the level achieved by BOOMERANG03[38]) - no effect from gain uncertainties was detected.

Polarization angle. Absolute errors in polarization angle can mix Q into U and thus E into B. SPIDER must measure the polarization angles (for each telescope) relatively precisely, but the level required is not difficult for a ground-based

measurement. This measurement is made much easier by the compact optics and correspondingly close "far field" of SPIDER; it can be done in a large highbay.

Relative detector pointing. Since, SPIDER does not rely on detector differencing to measure polarization; the rotating HWP eliminates sensitivity to relative detector pointing errors, which instead just cause an increase in the effective beamwidth of the observation after the signals from all detectors are averaged.

Absolute pointing. A common pointing error for both polarizations can cause E to B mixing. HHZ indicates that, for pointing uncertainties of less than 1% of the beam size (for SPIDER, less than $24''$ at 145GHz) the E-B contamination is much less than the lensing limit at all scales. SPIDER's pointing system is designed to achieve $6''$ accuracy, leading to the systematic error listed in Table 2.

Many other systematic effects (e.g. temperature drifts in the optics and cold stage, and common mode gain fluctuations), are enormously reduced by the rapid rotation of the HWP. An added virtue of the rapid HWP rotation is that every detector makes a full (Q,U) map of the sky it covers each night; this enables a multitude of detector-detector and day-to-day comparisons for systematic checks of the results.

8. CONCLUSION

SPIDER is an innovative approach to multi-frequency millimeter-wave polarization measurements on large angular scales. The payload design is simple and robust with strong emphasis placed on the control of systematic errors. SPIDER will map more than 50% of the sky each night over a 25 day flight. These observations will place strong constraints on the optical depth to reionization and the B-mode polarization signal from inflationary gravitational waves. In addition, SPIDER will provide large area maps of polarized dust emission at millimeter wavelengths.

SPIDER is already in fabrication in the U.S., Canada and the U.K. A test flight from North America is scheduled for 2008, and an LDB flight from Alice Springs, Australia in 2010, pending funding of proposals to NASA and to the Canadian Space Agency.

ACKNOWLEDGMENTS

We gratefully acknowledge Danny Ball and the staff at the Columbia Scientific Ballooning Facility for help in planning the flight strategy and performing payload flight simulations. Simulations of CMB observations were performed on the McKenzie cluster[64] at the Canadian Insitute for Theoretical Astrophysics which was funded by the Canada Foundation for Innovation and the Ontario Innovation Trust. CBN acknowledges sabbatical support from NASA JPL. Work on SPIDER at Caltech is currently funded by a generous gift from John Robinson.

REFERENCES

1. A. A. Penzias and R. W. Wilson, "A Measurement of Excess Antenna Temperature at 4080 Mc/s.," *Astrophys. J.* **142**, pp. 419–421, July 1965.
2. J. C. Mather, E. S. Cheng, D. A. Cottingham, R. E. Eplee, D. J. Fixsen, T. Hewagama, R. B. Isaacman, K. A. Jensen, S. S. Meyer, P. D. Noerdlinger, S. M. Read, L. P. Rosen, R. A. Shafer, E. L. Wright, C. L. Bennett, N. W. Boggess, M. G. Hauser, T. Kelsall, S. H. Moseley, R. F. Silverberg, G. F. Smoot, R. Weiss, and D. T. Wilkinson, "Measurement of the cosmic microwave background spectrum by the COBE FIRAS instrument," *Astrophys. J.* **420**, pp. 439–444, Jan. 1994.
3. D. J. Fixsen, E. S. Cheng, J. M. Gales, J. C. Mather, R. A. Shafer, and E. L. Wright, "The Cosmic Microwave Background Spectrum from the Full COBE FIRAS Data Set," *Astrophys. J.* **473**, pp. 576–587, Dec. 1996.
4. G. F. Smoot, C. L. Bennett, A. Kogut, E. L. Wright, J. Aymon, N. W. Boggess, E. S. Cheng, G. de Amici, S. Gulkis, M. G. Hauser, G. Hinshaw, P. D. Jackson, M. Janssen, E. Kaita, T. Kelsall, P. Keegstra, C. Lineweaver, K. Loewenstein, P. Lubin, J. Mather, S. S. Meyer, S. H. Moseley, T. Murdock, L. Rokke, R. F. Silverberg, L. Tenorio, R. Weiss, and D. T. Wilkinson, "Structure in the COBE differential microwave radiometer first-year maps," *Astrophys. J. Lett.* **396**, pp. L1–L5, Sept. 1992.
5. C. L. Bennett, A. J. Banday, K. M. Gorski, G. Hinshaw, P. Jackson, P. Keegstra, A. Kogut, G. F. Smoot, D. T. Wilkinson, and E. L. Wright, "Four-Year COBE DMR Cosmic Microwave Background Observations: Maps and Basic Results," *Astrophys. J. Lett.* **464**, p. L1, June 1996.

6. A. H. Guth, "Inflationary universe: A possible solution to the horizon and flatness problems," *Phys. Rev. D* **23**, pp. 347–356, Jan. 1981.
7. J. R. Bond, C. R. Contaldi, and D. Pogosyan, "Cosmic Microwave Background Snapshots: pre-WMAP and post-WMAP," *Philosophical Transactions Royal Society of London A* **361**, p. 2435, 2003.
8. C. MacTavish *et al.*, "Cosmological Parameters from the 2003 flight of BOOMERANG," *submitted to Astrophys. J.* , 2005. astro-ph/0507503.
9. D. N. Spergel *et al.*, "Wilkinson Microwave Anisotropy Probe (WMAP) Three Year Results: Implications for Cosmology," *submitted to Astrophys. J.* , 2006. astro-ph/0603449.
10. M. J. Rees, "Polarization and Spectrum of the Primeval Radiation in an Anisotropic Universe," *Astrophys. J. Lett.* **153**, pp. L1–L5, July 1968.
11. J. R. Bond and G. Efstathiou, "Cosmic background radiation anisotropies in universes dominated by nonbaryonic dark matter," *Astrophys. J. Lett.* **285**, pp. L45–L48, 1984.
12. J. M. Kovac, E. M. Leitch, C. Pryke, J. E. Carlstrom, N. W. Halverson, and W. L. Holzapfel, "Detection of polarization in the cosmic microwave background using DASI," *Nature* **420**, p. 772, December 2002. astro-ph/0209478.
13. E. Leitch *et al.*, "DASI Three-Year Cosmic Microwave Background Polarization Results," *submitted to Astrophys. J.* , 2004. astro-ph/0411122.
14. A. C. S. Readhead, S. T. Myers, T. J. Pearson, J. L. Sievers, B. S. Mason, C. R. Contaldi, J. R. Bond, R. Bustos, P. Altamirano, C. Achermann, L. Bronfman, J. E. Carlstrom, J. K. Cartwright, S. Casassus, C. Dickinson, W. L. Holzapfel, J. M. Kovac, E. M. Leitch, J. May, S. Padin, D. Pogosyan, M. Pospieszalski, C. Pryke, R. Reeves, M. C. Shepherd, and S. Torres, "Polarization Observations with the Cosmic Background Imager," *Science* **306**, pp. 836–844, Oct. 2004.
15. D. Barkats, C. Bischoff, P. Farese, L. Fitzpatrick, T. Gaier, J. O. Gundersen, M. M. Hedman, L. Hyatt, J. J. McMahon, D. Samtleben, S. T. Staggs, K. Vanderlinde, and B. Winstein, "First Measurements of the Polarization of the Cosmic Microwave Background Radiation at Small Angular Scales from CAPMAP," *Astrophys. J. Lett.* **619**, pp. L127–L130, Feb. 2005.
16. T. E. Montroy *et al.*, "A Measurement of the CMB $\langle EE \rangle$ Spectrum from the 2003 Flight of BOOMERANG," *submitted to Astrophys. J.* , 2005. astro-ph/0507514.
17. L. Page *et al.*, "Three-Year Wilkinson Microwave Anisotropy Probe (WMAP) Observations: Polarization Analysis," *submitted to Astrophys. J.* , *astro-ph/0603450* , 2006.
18. A. G. Polnarev, "Polarization and Anisotropy Induced in the Microwave Background by Cosmological Gravitational Waves," *Soviet Astro.* **29**, pp. 607–613, Dec. 1985.
19. R. Crittenden, R. L. Davis, and P. J. Steinhardt, "Polarization of the Microwave Background Due to Primordial Gravitational Waves," *Astrophys. J. Lett.* **417**, pp. L13–L16, Nov. 1993. astro-ph/9306027.
20. M. Zaldarriaga and U. Seljak, "All-sky analysis of polarization in the microwave background," *Phys. Rev. D* **55**, pp. 1830–1840, Feb. 1997.
21. M. Kamionkowski, A. Kosowsky, and A. Stebbins, "Statistics of cosmic microwave background polarization," *Phys. Rev. D* **55**, pp. 7368–7388, 1997.
22. U. Seljak and M. Zaldarriaga, "Signature of Gravity Waves in the Polarization of the Microwave Background," *Physical Review Letters* **78**, pp. 2054–2057, Mar. 1997. astro-ph/9609169.
23. M. S. Turner and M. White, "Dependence of inflationary reconstruction upon cosmological parameters," *Phys. Rev. D* **53**, pp. 6822–6828, June 1996.
24. M. Zaldarriaga and U. Seljak, "Gravitational lensing effect on cosmic microwave background polarization," *Phys. Rev. D* **58**, p. 23003 (6 pages), July 1998.
25. E. F. Bunn, M. Zaldarriaga, M. Tegmark, and A. de Oliveira-Costa, "E/B decomposition of finite pixelized CMB maps," *Phys. Rev. D* **67**, pp. 023501–+, Jan. 2003.
26. A. Lewis, A. Challinor, and N. Turok, "Analysis of CMB polarization on an incomplete sky," *Phys. Rev. D* **65**, pp. 023505–+, Jan. 2002. astro-ph/0106536.
27. C. R. Contaldi *et al. in preparation* , 2006.

28. P. Oxley, P. A. Ade, C. Baccigalupi, P. deBernardis, H. Cho, M. J. Devlin, S. Hanany, B. R. Johnson, T. Jones, A. T. Lee, T. Matsumura, A. D. Miller, M. Milligan, T. Renbarger, H. G. Spieler, R. Stompor, G. S. Tucker, and M. Zaldarriaga, "The EBEX experiment," in *Proceedings of the SPIE, Vol. 5498: Millimeter and Submillimeter Detectors for Astronomy II*, J. Zmuidzinas and W. S. Holland, ed., pp. 320–331, SPIE, (Bellingham, Washington), Oct. 2004.
29. S. Malhotra and J. E. Rhoads, "Luminosity Functions of Lyα Emitters at Redshifts z=6.5 and z=5.7: Evidence against Reionization at z$\leq$6.5," *Astrophys. J. Lett.* **617**, pp. L5–L8, Dec. 2004.
30. X. Fan *et al.*, "Constraining the Evolution of the Ionizing Background and the Epoch of Reionization with z 6 Quasars II: A Sample of 19 Quasars," *Astrophys. J. in press* , 2006. astro-ph/0512082.
31. T. Totani *et al.*, "Implications for the Cosmic Reionization from the Optical Afterglow Spectrum of the Gamma-Ray Burst 050904 at z = 6.3," *accepted by Pub. of the ASJ* , 2006. astro-ph/0512154.
32. A. Lewis, A. Challinor, and A. Lasenby, "Efficient Computation of Cosmic Microwave Background Anisotropies in Closed Friedmann-Robertson-Walker Models," *Astrophys. J.* **538**, pp. 473–476, Aug. 2000.
33. J. M. Lamarre, J. L. Puget, F. Bouchet, P. A. R. Ade, A. Benoit, J. P. Bernard, J. Bock, P. De Bernardis, J. Charra, F. Couchot, J. Delabrouille, G. Efstathiou, M. Giard, G. Guyot, A. Lange, B. Maffei, A. Murphy, F. Pajot, M. Piat, I. Ristorcelli, D. Santos, R. Sudiwala, J. F. Sygnet, J. P. Torre, V. Yurchenko, and D. Yvon, "The Planck High Frequency Instrument, a 3rd generation CMB experiment, and a full sky submillimeter survey," in *the proceedings of the workshop on "The Cosmic Microwave Background and its Polarization," New Astronomy Reviews*, S. Hanany and K. A. Olive, eds., Elsevier, 2003. astro-ph/0308075.
34. M. Sandri, M. Bersanelli, C. Burigana, R. C. Butler, F. Cuttaia, F. Finelli, E. Franceschi, A. Gruppuso, M. Malaspina, N. Mandolesi, A. Mennella, G. Morgante, G. Morigi, L. Popa, L. Terenzi, L. Valenziano, F. Villa, and LFI Consortium, "PLANCK Low Frequency Instrument: towards a final imaging of the CMB anisotropies," *Memorie della Societa Astronomica Italiana Supplement* **5**, pp. 411–+, 2004.
35. H. K. Eriksen, C. Dickinson, C. R. Lawrence, C. Baccigalupi, A. J. Banday, K. M. Gorski, F. K. Hansen, P. B. Lilje, E. Pierpaoli, M. D. Seiffert, K. M. Smith, and K. Vanderlinde. submitted to Astroph. J. astro-ph/0508268.
36. D. P. Finkbeiner, M. Davis, and D. J. Schlegel, "Extrapolation of galactic dust emission at 100 microns to cosmic microwave background radiation frequencies using firas," *Astrophys. J.* **524**, pp. 867–886, Oct. 1999.
37. J. Ruhl, P. A. R. Ade, J. E. Carlstrom, H.-M. Cho, T. Crawford, M. Dobbs, C. H. Greer, N. w. Halverson, W. L. Holzapfel, T. M. Lanting, A. T. Lee, E. M. Leitch, J. Leong, W. Lu, M. Lueker, J. Mehl, S. S. Meyer, J. J. Mohr, S. Padin, T. Plagge, C. Pryke, M. C. Runyan, D. Schwan, M. K. Sharp, H. Spieler, Z. Staniszewski, and A. A. Stark, "The South Pole Telescope," in *Astronomical Structures and Mechanisms Technology. Edited by Antebi, Joseph; Lemke, Dietrich. Proceedings of the SPIE, Volume 5498, pp. 11-29 (2004).*, J. Zmuidzinas, W. S. Holland, and S. Withington, eds., pp. 11–29, Oct. 2004.
38. S. Masi *et al.*, "Instrument, Method, Brightness and Polarization Maps from the 2003 flight of BOOMERanG," *submitted to Astr. & Astroph.* , 2005. astro-ph/0507509.
39. B. G. Keating, P. A. R. Ade, J. J. Bock, E. Hivon, W. L. Holzapfel, A. E. Lange, H. Nguyen, and K. Yoon, "BICEP: a large angular scale CMB polarimeter," in *Polarimetry in Astronomy. Edited by Silvano Fineschi. Proceedings of the SPIE, Volume 4843.*, pp. 284–295, Feb. 2003.
40. W. Hu, M. M. Hedman, and M. Zaldarriaga, "Benchmark parameters for CMB polarization experiments," *Phys. Rev. D* **67**, pp. 043004–+, Feb. 2003. astro-ph/0210096.
41. A. M. Title, "Improvement of Birefringent Filters. 2: Achromatic Waveplates," *Appl. Opt.* **14**, pp. 229–237, Jan. 1975.
42. S. Hanany *et al.*, "Millimeter-wave achromatic half-wave plate," *Appl. Opt.* **44**, pp. 4666–4670, 2005.
43. S. Hanany, T. Matsumura, B. Johnson, T. Jones, J. R. Hull, and K. B. Ma, "A Cosmic Microwave Background Radiation Polarimeter Using Superconducting Bearings," *IEEE Tran. Appl. Supercon.* **13**, pp. 2128–2133, 2003.
44. A. Goldin, J. J. Bock, C. Hunt, A. E. Lange, H. Leduc, A. Vayonakis, and J. Zmuidzinas, "SAMBA: Superconducting antenna-coupled, multi-frequency, bolometric array," *AIP Conf. Proc. 605: Low Temperature Detectors* **605**, pp. 251–254, 2002.
45. C. L. Kuo *et al.*, "Antenna-coupled TES bolometers for CMB polarimetry," in *Proceedings of the SPIE International Symposium on Astronomical Telescopes and Instrumentation*, 2006.
46. A. Vayonakis, C. Luo, H. G. Leduc, R. Schoelkopf, and J. Zmuidzinas, "The millimeter-wave properties of superconducting microstrip lines," *AIP Conf. Proc. 605: Low Temperature Detectors* **605**, pp. 539–542, 2002.

47. C. L. Hunt, J. J. Bock, P. K. Day, A. Goldin, A. E. Lange, H. G. LeDuc, A. Vayonakis, and J. Zmuidzinas, "Transition-edge superconducting antenna-coupled bolometer," in *Proceedings of the SPIE, Vol. 4855: Millimeter and Submillimeter Detectors for Astronomy*, T. G. Phillips and J. Zmuidzinas, ed., pp. 318–321, SPIE, (Bellingham, Washington), Feb. 2003.
48. C. L. Hunt. PhD thesis, California Institute of Technology, 2003.
49. K. D. Irwin, "An application of electrothermal feedback for high resolution cryogenic particle detection," *Appl. Phys. Lett.* **66**, pp. 1998–2000, 1995.
50. A. T. Lee, P. L. Richards, S. W. Nam, B. Cabrera, and K. D. Irwin, "A superconducting bolometer with strong electrothermal feedback," *Appl. Phys. Lett.* **69**, pp. 1801–1803, 1996.
51. S. Lee, J. M. Gildemeister, W. Holmes, A. T. Lee, and P. L. Richards, "Voltage-Biased Superconducting Transition-Edge Bolometer with Strong Electrothermal Feedback Operated at 370 mK," *Appl. Opt.* **37**, pp. 3391–3397, 1998.
52. J. M. Gildemeister, A. T. Lee, and P. L. Richards, "A fully lithographed voltage-biased superconducting spiderweb bolometer," *Appl. Phys. Lett.* **74**, pp. 868–870, 1999.
53. J. Blinchikoff and A. I. Zverev, *Filtering in the Time and Frequency Domains*, Wiley, New York, 1976.
54. K. D. Irwin, G. C. Hilton, J. M. Martinis, S. Deiker, N. Bergren, S. W. Nam, D. A. Rudman, and D. A. Wollman, "A Mo-Cu superconducting transition-edge microcalorimeter with 4.5 eV energy resolution at 6 keV," *Nucl. Instrum. Meth. A* **444**, pp. 184–187, 2000.
55. S. W. Deiker, W. Doriese, G. C. Hilton, K. D. Irwin, W. H. Rippard, J. N. Ullom, L. R. Vale, S. T. Ruggiero, A. Williams, and B. A. Young. to appear in Appl. Phys. Lett., 2005.
56. J. A. Chervenak, K. D. Irwin, E. N. Grossman, J. M. Martinis, C. D. Reintsema, and M. E. Huber, "Superconducting multiplexer for arrays of transition edge sensors," *Appl. Phys. Lett.* **74**, pp. 4043–4045, 1999.
57. P. A. J. de Korte, J. Beyer, S. Deiker, G. C. Hilton, K. D. Irwin, M. Macintosh, S. W. Nam, C. D. Reintsema, L. R. Vale, and M. E. Huber, "Time-division superconducting quantum interference device multiplexer for transition-edge sensors," *Rev. Sci. Instr.* **74**, pp. 3807–3815, Aug. 2003.
58. C. D. Reintsema, J. Beyer, S. W. Nam, S. Deiker, G. C. Hilton, K. Irwin, J. Martinis, J. Ullom, L. R. Vale, and M. Macintosh, "Prototype system for superconducting quantum interference device multiplexing of large-format transition-edge sensor arrays," *Rev. Sci. Instr.* **74**, pp. 4500–4508, 2003.
59. K. D. Irwin, M. D. Audley, J. A. Beall, J. Beyer, S. Deiker, W. Doriese, W. Duncan, G. C. Hilton, W. Holland, C. D. Reintsema, J. N. Ullom, L. R. Vale, and Y. Xu, "In-focal-plane SQUID multiplexer," *Nucl. Instrum. Meth. A* **520**, pp. 544–547, 2004.
60. W. S. Holland, W. Duncan, B. D. Kelly, K. D. Irwin, A. J. Walton, P. A. R. Ade, and E. I. Robson, "SCUBA-2: a new generation submillimeter imager for the James Clerk Maxwell Telescope," in *Millimeter and Submillimeter Detectors for Astronomy. Edited by Phillips, Thomas G.; Zmuidzinas, Jonas. Proceedings of the SPIE, Volume 4855, pp. 1-18 (2003).*, T. G. Phillips and J. Zmuidzinas, eds., pp. 1–18, Feb. 2003.
61. J. Bock, S. Church, M. Devlin, G. Hinshaw, A. Lange, A. Lee, L. Page, B. Partridge, J. Ruhl, M. Tegmark, P. Timbie, R. Weiss, B. Winstein, and M. Zaldarriaga, "Task Force on Cosmic Microwave Background Research," *ArXiv Astrophysics e-prints: astro-ph/0604101* , Apr. 2006.
62. W. Hu, M. M. Hedman, and M. Zaldarriaga, "Benchmark parameters for CMB polarization experiments," *Phys. Rev. D* **67**, pp. 043004–1–11, Feb. 2003.
63. N. Ponthieu, J. F. Macías-Pérez, M. Tristram, P. Ade, A. Amblard, R. Ansari, J. Aumont, É. Aubourg, A. Benoît, J.-P. Bernard, A. Blanchard, J. J. Bock, F. R. Bouchet, A. Bourrachot, P. Camus, J.-F. Cardoso, F. Couchot, P. de Bernardis, J. Delabrouille, F.-X. Désert, M. Douspis, L. Dumoulin, P. Filliatre, P. Fosalba, M. Giard, Y. Giraud-Héraud, R. Gispert, J. Grain, L. Guglielmi, J.-C. Hamilton, S. Hanany, S. Henrot-Versillé, J. Kaplan, G. Lagache, A. E. Lange, K. Madet, B. Maffei, S. Masi, F. Mayet, F. Nati, G. Patanchon, O. Perdereau, S. Plaszczynski, M. Piat, S. Prunet, J.-L. Puget, C. Renault, C. Rosset, D. Santos, D. Vibert, and D. Yvon, "Temperature and polarization angular power spectra of Galactic dust radiation at 353 GHz as measured by Archeops," *Astr. & Astroph.* **444**, pp. 327–336, Dec. 2005.
64. J. Dubinski, R. J. Humble, C. Loken, U.-L. Pen, and P. G. Martin, "McKenzie: A Teraflops Linux Beowulf Cluster for Computational Astrophysics," in *Proc. of the 17th Annual International Symposium on High Performance Computing Systems and Applications*,